Article:

eprints@whiterose.ac.uk
https://eprints.whiterose.ac.uk/

Maximal entanglement generation in spectrally distinct solid state qubits

Elena Callus[*] and Pieter Kok[†]

Department of Physics and Astronomy, The University of Sheffield, Sheffield, S3 7RH, UK

(Dated: February 25, 2021)

We demonstrate how to create maximal entanglement between two qubits that are encoded in two spectrally distinct solid-state quantum emitters embedded in a waveguide interferometer. The optical probe is provided by readily accessible squeezed light, generated by parametric down-conversion. By continuously probing the emitters, the photon scattering builds up entanglement with a concurrence that reaches its maximum after $O(10^1)$ photo-detection events. Our method does not require perfectly identical emitters, and accommodates spectral variations due to the fabrication process. It is also robust enough to create entanglement with a concurrence above 99% for 10% scattering photon loss, and can form the basis for practical entangled networks.

A key resource for quantum computing and quantum information processing is entanglement [1]. For quantum technologies that are implemented on a photonic platform, entanglement can be generated between spatially separated solid-state emitters, or artificial atoms, by embedding them in waveguides and allowing photons to interact with them. The generation of entanglement between artificial atoms has been well-addressed theoretically, and various schemes to entangle such qubits already exist [2–5]. These processes require only single- or few-photon interactions and a relatively simple setup with few optical components, and utilise "which-path" information erasure. However, these schemes require the use of qubits that are spectrally identical, necessary for coherent erasure of path information, and therefore any frequency variations between the emitters would result in degraded entanglement. Considering that current fabrication processes of solid-state emitters result in spectrally inhomogeneous samples [6], the matching of sufficiently similar qubits adds a large overhead cost and the entanglement process cannot occur on a large-scale. Although methods such as diameter tuning [7] and strain tuning [8] can be used to tune the frequencies of the emitters, they require additional technical complexity in the experimental setup. Furthermore, these techniques are applicable only for sufficiently similar emitters and generally cannot be used for arbitrary pairings.

In order to try and overcome this practical limitation, Hurst *et al.* [9] considered how spectral variation in emitters affects the entanglement outcome and demonstrated that this inhomogeneity is not as hindering as previously thought. They propose a simple setup involving linear optics and show that it is possible to attain entanglement deterministically for certain combinations of central energies and line-widths by adjusting the frequency of the probing photons. One drawback of the setup is that it requires the use of two-mode Fock states, $|n, m\rangle$, which are typically not easily accessible given current technologies. Also, for a given Fock state, near-perfect entanglement is attained only for certain ranges of central energy and line-width combinations. This necessitates the use of increasingly hard to source higher-order Fock states in

order to entangle certain regimes of emitter-pairings.

In this paper, we show that two spectrally different emitters can be entangled with extremely high concurrence in a nearly deterministic manner by repeatedly probing the emitters with squeezed light, generated by means of spontaneous parametric down-conversion (SPDC) [10]. This brings us one step closer to a physical implementation, given the accessibility of squeezed light [11], and further eases restrictions when it comes to the matching of inhomogeneous solid-state emitters. In addition, we take into consideration photon loss during the scattering process and show that very high concurrence is still possible in non-ideal situations.

The setup consists of a waveguide Mach-Zehnder interferometer (MZI) with a 50:50 beam splitter at either end, and solid-state emitters, acting as our logical qubits, embedded in each arm (see Fig. 1). The emitters have two long-lived low-lying spin states, $|\uparrow\rangle$ and $|\downarrow\rangle$, and an excited state $|e\rangle$, and are of the L-configuration, with the excited state coupled to only one of the spin states (say, the $|\uparrow\rangle$ state). The transition between the other spin state and the excited state is forbidden by polarisation selection rules. Each qubit is prepared in the superposition state $(|\uparrow\rangle + |\downarrow\rangle)/\sqrt{2}$. To ensure that photons are scattered only in the forward direction, the two emitters are placed at so-called *c-points* in the waveguide. These are
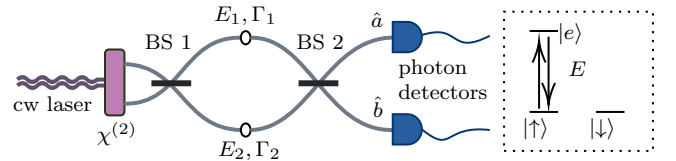
FIG. 1. Schematic of the setup: the squeezed light generated by a $\chi^{(2)}$ nonlinear crystal driven by a continuous-wave laser pump enters the Mach-Zehnder interferometer, where it scatters off the two solid-state emitters characterised by energies and line-widths E_1, Γ_1 and E_2, Γ_2. The photon measurement is made at the interferometer output, with the mode operators $\hat{a}$ and $\hat{b}$ representing the output arms. Inset shows the L-configuration of the emitters, with the $|\uparrow\rangle$ state coupled to the excited state, $|e\rangle$, and transition energy $E = E_1$, E_2.

the locations where emitters exhibit highly directional scattering of circularly polarized light due to the spatial confinement of the electromagnetic field [12]. High levels of directional scattering have been observed experimentally [12–14]. Finally, we have photon detectors placed at both output arms of the MZI, where the state of the emitters post-scattering is heralded by the photon detection signature. We assume that the photon detectors have near-perfect efficiency [15, 16].

For emitters at c-points, the transmission coefficient for a photon of frequency ω scattering off a two-level emitter is obtained from the single photon S-matrix, and is given by [17]

$$t(\omega) = \frac{\hbar\omega - E - \mathrm{i}\hbar\left(\Gamma - \gamma\right)/2}{\hbar\omega - E + \mathrm{i}\hbar\left(\Gamma + \gamma\right)/2}, \tag{1}$$

where E is the transition frequency of the emitter, and Γ and γ are the coupling rates of the emitter to the waveguide and the non-guided modes, respectively.

In the case of zero photon loss, $\gamma = 0$ and the scattered photon acquires a pure phase shift. In the ideal case, the two solid-state emitters are identical in their energies and line-widths and their spin states are entangled by passing a resonant probe photon through the interferometer. After interfering with the first beamsplitter, the photon scatters off the emitters and acquires a π phase shift from its interaction with the $|\uparrow\rangle$ state [18, 19], whilst the state $|\downarrow\rangle$ leaves the photon unchanged. The resulting state of the qubits and the probe photon after the second beam splitter is given by $(|\Phi^-\rangle \otimes |1,0\rangle - |\Psi^-\rangle \otimes |0,1\rangle)/\sqrt{2}$, where $|\Phi^-\rangle = (|\uparrow\uparrow\rangle - |\downarrow\downarrow\rangle)/\sqrt{2}$, $|\Psi^-\rangle = (|\uparrow\downarrow\rangle - |\downarrow\uparrow\rangle)/\sqrt{2}$, and $|1,0\rangle$ and $|0,1\rangle$ represent the two possible photon-detection outcomes. Therefore, either photon measurement outcome would result in a maximally entangled bipartite state. However, if we deviate from identical solid-state emitters and allow for spectral variations between the two, we do not obtain a maximally entangled state. Here, the amount of generated entanglement can be tuned by adjusting the frequency of the photon probe.

We consider the two-mode squeezed vacuum as our input state, routinely generated by spontaneous parametric down-conversion (SPDC) in a nonlinear $\chi^{(2)}$ crystal driven by a continuous-wave (CW) pump laser. During the SPDC process, a pump photon of frequency ω_p is annihilated and a signal and idler photon, with frequencies ω_s and ω_i, respectively, are created. When the pump laser is on resonance with the crystal, the squeezing operator is given by $S(\xi) = \exp[\frac{1}{2}(\xi^*\hat{a}\hat{b} - \xi\hat{a}^\dagger\hat{b}^\dagger)]$ [20], where $\hat{a}$, $\hat{b}$ are the mode operators for the two input arms of the MZI. When acting on vacuum, the squeezing operator generates the state [21]

$$|\psi\rangle = \frac{1}{\cosh r} \sum_{n=0}^{\infty} (-\mathrm{e}^{\mathrm{i}\phi}\tanh r)^n \frac{(\hat{a}^\dagger\hat{b}^\dagger)^n}{n!} |0\rangle, \tag{2}$$

where $\xi = r\mathrm{e}^{\mathrm{i}\phi}$ is determined by the material properties and the laser pump. We can ignore vacuum contributions

since they do not affect the state of the multi-partite system in any way. We also neglect higher order photon pair production in the SPDC process as this occurs rarely; for typical experimental parameters and utilising a CW pump, the generation of multi-pair states as a fraction of single biphotons is of the order of 10^{-8} per Watt of pump power [22]. This places an upper limit to how strong the crystal can be pumped before multiple pair production changes the dynamics of the protocol. The low conversion efficiency in SPDC is due to the relative weakness of the signal and idler fields relative to the pump field [23]. For a thin SPDC crystal, the single biphoton state can be expressed as [24, 25]

$$|\psi\rangle = \int \mathrm{d}\omega_s\, \mathrm{d}\omega_i\, \mathcal{E}_p(\omega_s + \omega_i)\Psi(k_s + k_i - k_p)$$
$$\times \hat{a}^\dagger(\omega_s, k_s)\hat{b}^\dagger(\omega_i, k_i) |0\rangle, \tag{3}$$

where the envelope of the pump laser $\mathcal{E}_p$ and wave number correlation function Ψ are a direct consequence of phase-matching conditions relating to the conservation of energy and momentum, respectively, in the crystal.

We require that the photons are quasi-monochromatic, which can be achieved by either using a monochromatic pump beam, or by frequency filtering post-SPDC. For quasi-monochromatic photons, the non-linear term in the S-matrix from two-photon scattering becomes negligible and the process can be described linearly, where the total phase shift accumulated during the interaction is the sum of the phase shifts imparted by the individual photons. Additionally, photons with a broader bandwidth are more likely to excite the emitter due to their shorter temporal length, which may result in undesirable spontaneous emission [9].

In order to successfully reach maximal entanglement, the down-conversion process needs to be degenerate, i.e., producing signal and idler photons with the same frequency. A frequency difference between the signal and idler photons would impart which-path information during the scattering process, as the total acquired phase-shift is stronger for one emitter than the other (assuming non-identical emitters). The frequency of the generated photons needs to be optimised for the central energies and line-widths of the two quantum emitters. The phase shift imparted by the photons affects the interference at the second beam splitter and, consequently, the final state of the light-matter system. In order to successfully build up entanglement, we require $t_1^2(\omega) = t_2^2(\omega)$, where $t_i(\omega)$ is the transmission coefficient for the scattering in arm i. The frequency of the probe photons, therefore, needs to satisfy either of the following:

$$\hbar\omega = \frac{1}{2}\left[E_1 + E_2 \pm \sqrt{(E_1 - E_2)^2 - \hbar^2\Gamma_1\Gamma_2}\right], \tag{4a}$$

$$\text{or} \qquad \hbar\omega = \frac{E_2\Gamma_1 - E_1\Gamma_2}{\Gamma_1 - \Gamma_2}, \tag{4b}$$

where E_1 and E_2 are the energies of the emitters, and Γ_1 and Γ_2 are their line-widths, respectively [see Supplemental Material (SM) for more details [26]].

Next, we consider the state of the system after N detection events. Let m be the number of events where both detectors register a photon and n be the number of events where the two photons reach the same detector, with $N = m + n$. Then the state of the system after the $(N + 1)^{\text{th}}$ probe and right before photon-detection can be expressed as

$$\begin{aligned}
|\psi_{m,n}\rangle = \frac{1}{4c_{m,n}} &\left[(1 + t_1^2(\omega))^m (t_1^2(\omega) - 1)^{n+1} |{\uparrow\downarrow}\rangle + (1 + t_2^2(\omega))^m (1 - t_2^2(\omega))^{n+1} |{\downarrow\uparrow}\rangle \right] \otimes \left[\left(\hat{a}^\dagger\right)^2 + \left(\hat{b}^\dagger\right)^2 \right] |0\rangle \\
+ \frac{1}{2c_{m,n}} &\left[(t_1^2(\omega) + t_2^2(\omega))^{m+1} 0^n |{\uparrow\uparrow}\rangle + (1 + t_1^2(\omega))^{m+1}(t_1^2(\omega) - 1)^n |{\uparrow\downarrow}\rangle \right. \\
&\left. + (1 + t_2^2(\omega))^{m+1}(1 - t_2^2(\omega))^n |{\downarrow\uparrow}\rangle + 2^{m+1} 0^n |{\downarrow\downarrow}\rangle \right] \otimes \hat{a}^\dagger \hat{b}^\dagger |0\rangle \, ,
\end{aligned} \tag{5}$$

where $c_{m,n}$ is the respective normalization constant [see SM for more details [26]]. Post-selecting on the photon detection, we obtain the heralded state of the emitters. Given that there is no information about which emitter has gained a phase shift, some of the which-path information of each photon is erased, resulting in a cumulative entanglement gain.

We characterize the amount of entanglement for the two-qubit state post-photon detection, ρ, using the concurrence, $\mathcal{C}(\rho)$ [27]. Fig. 2 shows how the concurrence of two non-identical emitters can reach unity by repeatedly sending in photon pairs at the optimal frequency [Eq. (4)] and keeping track of the photon detection signature. Perfect entanglement is achieved regardless of the photon detection signature, and there is no need to reject samples on the basis of certain measurement outcomes. Furthermore, the process does not destroy any generated entanglement. Instead, in the case where there has been at least one coincident photon detection, further probing will toggle the state of the qubits between $|\Psi^+\rangle$ and $|\Psi^-\rangle$, where $|\Psi^\pm\rangle = (|{\uparrow\downarrow}\rangle \pm |{\downarrow\uparrow}\rangle)/\sqrt{2}$. Otherwise, if photons are registered by just one of the detectors at every iteration, the qubits keep approaching the maximally entangled state $(|{\uparrow\uparrow}\rangle + \exp(\mathrm{i}\phi)|{\downarrow\downarrow}\rangle)/\sqrt{2}$, where ϕ is a cumulative phase determined by $t_1(\omega)$ and $t_2(\omega)$.

The number of iterations needed to ensure that perfect entanglement has been reached is closely related to the average concurrence after the first iteration, weighted by the photon outcome probabilities, which in turn depends on the ratio of the line-widths of the two emitters as well as the detuning of their central energies. The trajectories in Fig. 2 show the random process of how the concurrence is updated after each photo-detection event. The measurement process is characterised by a projection operator, assuming perfect photon counters. The scattering process is then repeated, where the state of the qubits is now the reduced density matrix after the previous measurement projection. Given a quasi-mono-chromatic probe photon and zero photon loss, the (reduced) density matrix of the two emitters remains pure.

In some situations, such as those shown in Fig. 2, it may be desirable to pair emitters with larger spectral variations in order to maximally entangle in fewer detection events without needing to consider the detector signatures. In the case of emitter pairings where the initial average concurrence is low, it is still possible to obtain maximal entanglement within fewer detection events, albeit with a lower probability, by considering the detector signatures; the concurrence reaches unity when both photons reach the same detector. This can be seen in the first line of Eq. (5), where such an outcome would result in the Bell state $|\Psi^\pm\rangle = \frac{1}{\sqrt{2}}(|{\uparrow\downarrow}\rangle \pm |{\downarrow\uparrow}\rangle)$ (up to some overall phase). When the emitters are identical, both scattering events in the two arms impart similar phases, which leads to a very high probability of detection coincidences in the output. In this situation, the amount of entanglement generated is negligble. When two photons are found in the same detector, the concurrence jumps to unity. Therefore, we find the remarkable property that more dissimilar emitters can produce entanglement at a faster rate. There are regimes of δ/Γ_1 and Γ_2/Γ_1 where mere dissimilarity is not sufficient, but the range of emitters that can be entangled efficiently is vastly larger than when we require that all emitters are identical.

We now consider photon loss during the scattering interaction at either emitter, which negatively impacts the entanglement process (we still assume near-perfect photon detection efficiency). The β-factor is defined as the coupling to the non-guided modes (i.e., modes resulting in loss to the environment) as a fraction of the total field coupling, $\beta = \Gamma/(\Gamma + \gamma)$. Once we introduce photon loss to our system, describing the scattering process becomes more involved as the photon in the guided mode will not only obtain a phase shift, but will also undergo a change in the probability amplitude (since γ is no longer zero). The transmission coefficient of the photon that is lost to
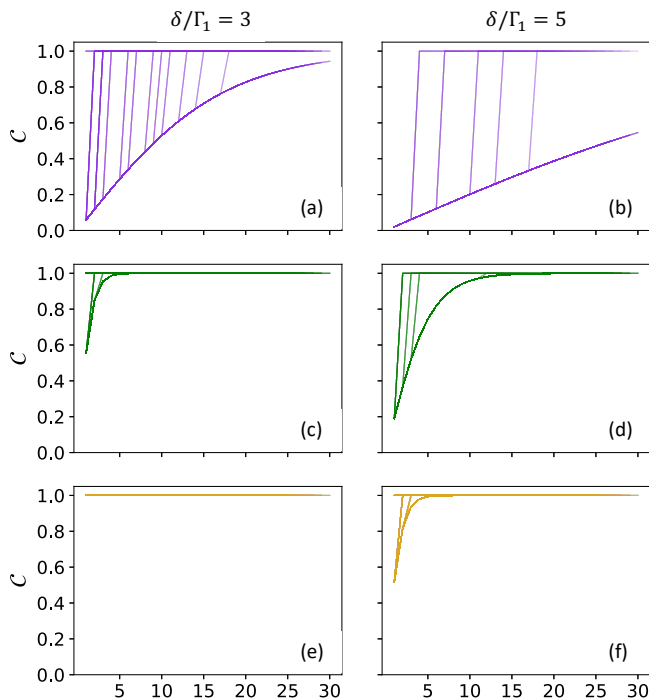
FIG. 2. Typical concurrence trajectories given a series of photon detection events (horizontal axis) for the lossless case ($\gamma = 0$). Γ_1 and Γ_2 are the emitter line-widths, and the central energy detuning between the two emitters is $\delta = |E_2 - E_1|$. Here, $\delta/\Gamma_1 = 3$ (left column) and 5 (right column), and Γ_2/Γ_1 is set to 1 [(a) and (b)], 3 [(c) and (d)] and 5 [(e) and (f)]. We observe that within some spectral parameters, more dissimilar emitters can produce entanglement at a faster rate.

the environment is given by [28]

$$t_e(\omega) = \frac{-i\hbar\sqrt{\Gamma\gamma}}{\hbar\omega - E + i\hbar\left(\Gamma + \gamma\right)/2}. \quad (6)$$

One way to overcome the consequences of scattering losses is to consider photon number resolving detectors and discard samples where photon loss has occured. However, given that such detectors types are still in the experimental stage, we consider non-number resolving detectors in our calculations. The methodology for generating the trajectories is the same as for $\beta = 1$, but we will find that the qubits are in a mixed state post-photon detection. For emitter matches that reach perfect entanglement rapidly in the lossless case, it is possible to obtain over 99% concurrence within a few iterations for $\beta \sim 0.9$.

In order to achieve the best concurrence, we include a bit flip operation on both emitters (in the computational basis) after every detection event. The scattering process results in an uneven accumulation of probability amplitudes on $|\uparrow\uparrow\rangle$ and $|\downarrow\downarrow\rangle$, and $|\uparrow\downarrow\rangle$ and $|\downarrow\uparrow\rangle$ due to γ no longer being zero [see SM for more details [26]]. Performing a bit flip balances out the probability amplitudes of these spin states and improves the amount of possible
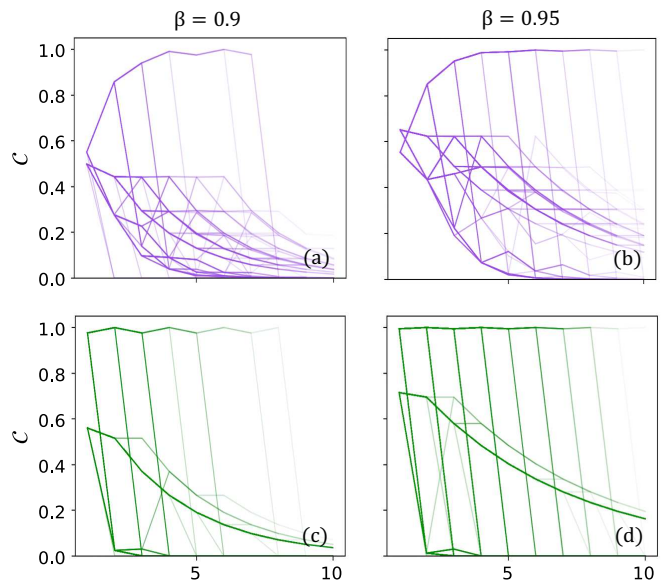

FIG. 3. Typical concurrence trajectories given a series of photon detection events for $\beta = 0.9$ (left column) and $\beta = 0.95$ (right column). Γ_1 and Γ_2 are the emitter line-widths, and $\delta = |E_2 - E_1|$ is the central energy detuning between the two emitters. Here, $\delta/\Gamma_1 = 3$, $\Gamma_2/\Gamma_1 = 3$ [(a) and (b)], and $\Gamma_2/\Gamma_1 = 5$ [(c) and (d)]. The horizontal axis includes both successful photon-detection events and zero-photon detections due to scattering losses.

entanglement generation. Fig. 3 shows random concurrence trajectories for the $\beta < 1$ case, where zero-photon detection outcomes due to scattering losses are accounted for. The plots demonstrate that the iterative process can generate near-perfect entanglement, where the probability of obtaining concurrence $C > 0.99$ within the first 10 iterations is $10-50\%$ for the shown configurations. This occurs after several simultaneous photon measurements at both detectors.

Next, we address challenges to the physical implementation of the proposed scheme. We have seen how photon loss degrades the entanglement generation process and decreases the rate at which samples can be successfully entangled. However, the results can be improved by implementing a bit-flip after every photon detection event. Alternatively, one can make use of photon-number-resolving detectors and discard samples where a photon is lost.

Another physical issue that needs to be taken into account is the finite coherence time of the solid-state emitters, which is affected by mechanisms such as the spin-orbit and nuclear-spin interactions [29]. For semiconductor quantum dots, this coherence time is relatively short, ranging between > 100 ns and several microseconds [30–33]. For nitrogen-vacancy centres in diamond, the coherence time can be in the millisecond range [34–36], and exceeding half a second when enhanced by means of decoupling pulsing to suppress the spin decoherence
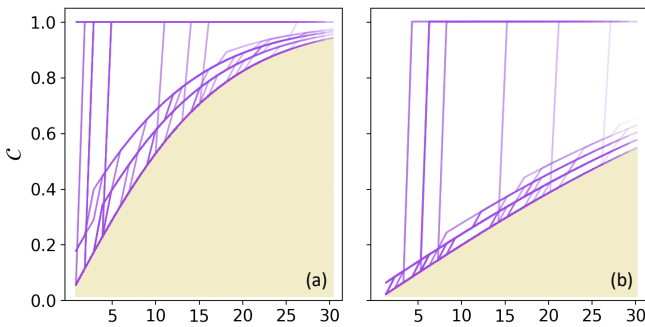
FIG. 4. Typical concurrence trajectories given a series of photon detection events (horizontal axis) for the lossless case ($\gamma = 0$) when probing with both $|1, 1\rangle$ and $|2, 2\rangle$ states, where $|2, 2\rangle$ states occur $\sim 15\%$ of the time. Here, $\delta/\Gamma_1 = 3$ (a) and 5 (b), Γ_2/Γ_1 is set to 1, and the photon detectors are assumed to be number-resolving. The shaded region represents the area under the curve in Fig. 2. This shows that higher-order pair production in the down-conversion process is not detrimental to entanglement generation.

[37]. The emitters must survive long enough for the entanglement generation to take place. This means that SPDC in the weak photon generation limit may be too slow. Strong pump amplitudes will create multiple pairs, however, and we must take into account the effect of four-photon scattering. Fig. 4 compares the concurrence of the emitters when probing with just single biphoton states (i.e., $|1, 1\rangle$) with possible higher-order pair production, using photon-number resolving detectors. The generation of multi-biphoton states does not disrupt the entanglement generation process, but rather may enhance it.

In conclusion, we have presented a way to maximally entangle two solid-state quantum emitters via a cumulative entanglement generation protocol, taking into consideration the inhomogeneity arising from the fabrication process. Our protocol does not require that we discard entanglement due to undesired photon detection outcomes. We also have accounted for scattering photon losses and show that the results are still promising: for certain emitter pairings, it is still possible to create entanglement with a concurrence of > 0.99 and $< 10\%$ scattering losses within a small number of photon-detection events. Additionally, the setup is relatively simple and can be implemented using current technology. We find that in trying to generate entanglement, we have more flexibility than previously thought; in fact, larger energy detuning or line-width variations might result in faster entanglement generation with higher concurrence, bringing us closer to solid state entanglement as a viable technology for quantum information processing.

* ecallus1@sheffield.ac.uk
† p.kok@sheffield.ac.uk

[1] R. Jozsa and N. Linden, Proceedings of the Royal Society of London. Series A: Mathematical, Physical and Engineering Sciences **459**, 2011 (2003), quant-ph/0201143.

[2] S. D. Barrett and P. Kok, Physical Review A **71**, 060310 (2005), quant-ph/0408040.

[3] C. Cabrillo, J. I. Cirac, P. García-Fernández, and P. Zoller, Physical Review A **59**, 1025 (1999), quant-ph/9810013.

[4] S. Bose, P. L. Knight, M. B. Plenio, and V. Vedral, Physical Review Letters **83**, 5158 (1999), quant-ph/9908004.

[5] L.-M. Duan and H. J. Kimble, Physical Review Letters **90**, 253601 (2003), quant-ph/0301164.

[6] Y. Arakawa and M. J. Holmes, Applied Physics Reviews **7**, 021309 (2020).

[7] T. Heuser, J. Große, A. Kaganskiy, D. Brunner, and S. Reitzenstein, APL Photonics **3**, 116103 (2018).

[8] L. Zhai, M. C. Löbl, J.-P. Jahn, Y. Huo, P. Treutlein, O. G. Schmidt, A. Rastelli, and R. J. Warburton, Applied Physics Letters **117**, 083106 (2020), 2008.11735.

[9] D. L. Hurst, K. B. Joanesarson, J. Iles-Smith, J. Mork, and P. Kok, Physical Review Letters **123**, 023603 (2019), 1901.03631.

[10] P. J. Mosley, J. S. Lundeen, B. J. Smith, and I. A. Walmsley, New Journal of Physics **10**, 093011 (2008), 0807.1409.

[11] U. L. Andersen, T. Gehring, C. Marquardt, and G. Leuchs, Physica Scripta **91**, 053001 (2016), 1511.03250.

[12] R. J. Coles, D. M. Price, J. E. Dixon, B. Royall, E. Clarke, P. Kok, M. S. Skolnick, A. M. Fox, and M. N. Makhonin, Nature Communications **7**, 11183 (2016), 1506.02266.

[13] P. Lodahl, S. Mahmoodian, S. Stobbe, A. Rauschenbeutel, P. Schneeweiss, J. Volz, H. Pichler, and P. Zoller, Nature **541**, 473 (2017), 1608.00446.

[14] B. Lang, D. M. Beggs, and R. Oulton, Philosophical Transactions of the Royal Society A: Mathematical, Physical and Engineering Sciences **374**, 20150263 (2016), 1601.04591.

[15] A. E. Lita, A. J. Miller, and S. W. Nam, Optics Express **16**, 3032 (2008).

[16] D. Fukuda, G. Fujii, T. Numata, K. Amemiya, A. Yoshizawa, H. Tsuchida, H. Fujino, H. Ishii, T. Itatani, S. Inoue, and T. Zama, Optics Express **19**, 870 (2011).

[17] J.-T. Shen and S. Fan, Physical Review A **76**, 062709 (2007).

[18] A. Nysteen, D. P. S. McCutcheon, M. Heuck, J. Mørk, and D. R. Englund, Physical Review A **95**, 062304 (2017), 1612.04803.

[19] S. Fan, Ş. E. Kocabaş, and J.-T. Shen, Physical Review A **82**, 063821 (2010), 1011.3296.

[20] H. Seifoory, S. Doutre, M. M. Dignam, and J. E. Sipe, Journal of the Optical Society of America B **34**, 1587 (2017).

[21] B. L. Pieter Kok, Introduction to Optical Quantum Information (Cambridge University Press, 2010).

[22] J. Schneeloch, S. H. Knarr, D. F. Bogorin, M. L. Levangie, C. C. Tison, R. Frank, G. A. Howland, M. L.

Fanto, and P. M. Alsing, Journal of Optics **21**, 043501 (2019), 1807.10885.

[23] C. Couteau, Contemporary Physics **59**, 291 (2018), 1809.00127.

[24] S.-Y. Baek and Y.-H. Kim, Physical Review A **77**, 043807 (2008).

[25] O. Kwon, Y.-S. Ra, and Y.-H. Kim, Optics Express **17**, 13059 (2009).

[26] .

[27] S. Hill and W. K. Wootters, Physical Review Letters **78**, 5022 (1997), quant-ph/9703041.

[28] E. Rephaeli and S. Fan, Photonics Research **1**, 110 (2013).

[29] J. Fischer, M. Trif, W. Coish, and D. Loss, Solid State Communications **149**, 1443 (2009), 0903.0527.

[30] J. Yoneda, K. Takeda, T. Otsuka, T. Nakajima, M. R. Delbecq, G. Allison, T. Honda, T. Kodera, S. Oda, Y. Hoshi, N. Usami, K. M. Itoh, and S. Tarucha, Nature Nanotechnology **13**, 102 (2018), 1708.01454.

[31] J. H. Prechtel, A. V. Kuhlmann, J. Houel, A. Ludwig, S. R. Valentin, A. D. Wieck, and R. J. Warburton, Nature Materials **15**, 981 (2016).

[32] J. Houel, J. H. Prechtel, A. V. Kuhlmann, D. Brunner, C. E. Kuklewicz, B. D. Gerardot, N. G. Stoltz, P. M. Petroff, and R. J. Warburton, Physical Review Letters **112**, 107401 (2014), 1307.2000.

[33] J. R. Petta, A. C. Johnson, J. M. Taylor, E. A. Laird, A. Yacoby, M. D. Lukin, C. M. Marcus, M. P. Hanson, and A. C. Gossard, Science **309**, 2180 (2005).

[34] E. D. Herbschleb, H. Kato, Y. Maruyama, T. Danjo, T. Makino, S. Yamasaki, I. Ohki, K. Hayashi, H. Morishita, M. Fujiwara, and N. Mizuochi, Nature Communications **10**, 3766 (2019).

[35] J. M. Zadrozny, J. Niklas, O. G. Poluektov, and D. E. Freedman, ACS Central Science **1**, 488 (2015).

[36] K. D. Jahnke, B. Naydenov, T. Teraji, S. Koizumi, T. Umeda, J. Isoya, and F. Jelezko, Applied Physics Letters **101**, 012405 (2012), 1206.4260.

[37] N. Bar-Gill, L. Pham, A. Jarmola, D. Budker, and R. Walsworth, Nature Communications **4**, 1743 (2013), 1211.7094.

[38] W. K. Wootters, Physical Review Letters **80**, 2245 (1998), quant-ph/9709029.

SUPPLEMENTAL MATERIAL: MAXIMAL ENTANGLEMENT GENERATION IN SPECTRALLY DISTINCT SOLID STATE QUBITS

Scattering amplitudes

The scattering coefficient gained by a photon (upon scattering to a guided mode) is [19]

$$t(\omega) = \frac{\hbar\omega - E - \mathrm{i}\hbar(\Gamma - \gamma)/2}{\hbar\omega - E + \mathrm{i}\hbar(\Gamma + \gamma)/2}, \tag{SM.1}$$

where E is the transition energy of the emitter, and Γ and γ are the coupling rates to the guided and non-guided modes, respectively. When a photon is lost to the environment upon scattering, it gains a probability amplitude given by [28]

$$t_e(\omega) = \frac{-\mathrm{i}\hbar\sqrt{\Gamma\gamma}}{\hbar\omega - E + \mathrm{i}\hbar(\Gamma + \gamma)/2}. \tag{SM.2}$$

In the case of two-photon scattering, the scattering is characterised by a linear term and a bound state term. For the zero-, one- and two-photon loss cases, the post-scattering wavefunctions become [28]

$$\begin{aligned}
\tilde{\beta}(\omega_1, \omega_2) =& \frac{1}{2}t(\omega_1)t(\omega_2)\left[\beta(\omega_1, \omega_2) + \beta(\omega_2, \omega_1)\right] \\
&+ \frac{\mathrm{i}\sqrt{\Gamma}}{2\pi}s(\omega_1)s(\omega_2)\int \mathrm{d}k\left[s(k) + s(\omega_1 + \omega_2 - k)\right]\beta(k, \omega_1 + \omega_2 - k),
\end{aligned} \tag{SM.3}$$

$$\begin{aligned}
\tilde{\beta}_e(\omega_1, \omega_2) =& t(\omega_1)t_e(\omega_2)\beta(\omega_1, \omega_2) + t_e(\omega_1)t(\omega_2)\beta(\omega_2, \omega_1) \\
&+ \frac{\sqrt{\Gamma}}{\pi}s(\omega_1)s_e(\omega_2)\int \mathrm{d}k\left[s(k) + s(\omega_1 + \omega_2 - k)\right]\beta(k, \omega_1 + \omega_2 - k),
\end{aligned} \tag{SM.4}$$

and

$$\begin{aligned}
\tilde{\beta}_{ee}(\omega_1, \omega_2) =& \frac{1}{2}t_e(\omega_1)t_e(\omega_2)\left[\beta(\omega_1, \omega_2) + \beta(\omega_2, \omega_1)\right] \\
&+ \frac{\mathrm{i}\sqrt{\Gamma}}{2\pi}s_e(\omega_1)s_e(\omega_2)\int \mathrm{d}k\left[s(k) + s(\omega_1 + \omega_2 - k)\right]\beta(k, \omega_1 + \omega_2 - k),
\end{aligned} \tag{SM.5}$$

respectively, where $\beta(\omega_1, \omega_2)$ is the original wavepacket, such that $\int \mathrm{d}\omega_1\, \mathrm{d}\omega_2\, |\beta(\omega_1, \omega_2)| = 1$, and

$$s(\omega) = \frac{\hbar\sqrt{\Gamma}}{\hbar\omega - E + \mathrm{i}\hbar(\Gamma + \gamma)/2}, \tag{SM.6}$$

$$s_e(\omega) = \frac{\hbar\sqrt{\gamma}}{\hbar\omega - E + \mathrm{i}\hbar(\Gamma + \gamma)/2}. \tag{SM.7}$$

Since we consider identical monochromatic photons where $\beta(\omega_1, \omega_2) = \delta(\omega_1 - \omega)\delta(\omega_2 - \omega)$, the integral of the bound state term vanishes. This is because monochromatic photons have an infinite temporal spread and therefore do not excite the emitter, resulting in no spontaneous emission since the emitter remains in the ground state (indeed, the term $s(\omega)$ is related to the spontaneous emission of the emitter into the waveguide [19]).

Integrating the post-scattering wavefunctions for the monochromatic case, the scattering amplitudes simplify to

$$\int \mathrm{d}\omega_1\, \mathrm{d}\omega_2\, \tilde{\beta}(\omega_1, \omega_2) = t(\omega)^2, \tag{SM.8}$$

$$\int \mathrm{d}\omega_1\, \mathrm{d}\omega_2\, \tilde{\beta}_e(\omega_1, \omega_2) = 2t(\omega)t_e(\omega), \tag{SM.9}$$

$$\int \mathrm{d}\omega_1\, \mathrm{d}\omega_2\, \tilde{\beta}_{ee}(\omega_1, \omega_2) = t_e(\omega)^2. \tag{SM.10}$$

Emitter density matrix

Zero photon-loss case ($\beta = 1$)

In the case of no photon losses, the post-measurement state of the qubit remains pure, regardless of the detection outcome. This is due to our choice of using a single frequency biphoton state and the absence of scattering losses – each detection measurement corresponds to a single projection measurement. (Note that this no longer holds when using higher order biphoton states.) We therefore can make use of the usual wavefunction and ket notation to obtain a general expression for the state of the qubits after any number of photon-measurement events.

We start with both emitters in the state $\frac{1}{\sqrt{2}}(|\uparrow\rangle + |\downarrow\rangle)$, giving an initial state

$$|\psi_1\rangle = \frac{1}{2}(|\uparrow\rangle + |\downarrow\rangle) \otimes (|\uparrow\rangle + |\downarrow\rangle) \otimes \hat{a}^\dagger \hat{b}^\dagger |0\rangle, \tag{SM.11}$$

where $\hat{a}^\dagger$ and $\hat{b}^\dagger$ are the creation operators for the upper and lower input arms of the interferometer, both with frequency ω.

The state after the first beam-splitter ($\hat{a} \to \frac{1}{\sqrt{2}}(\hat{a} + \hat{b})$ and $\hat{b} \to \frac{1}{\sqrt{2}}(\hat{a} - \hat{b})$) is

$$\begin{aligned}|\psi_2\rangle &= \frac{1}{4}(|\uparrow\rangle + |\downarrow\rangle) \otimes (|\uparrow\rangle + |\downarrow\rangle) \otimes (\hat{a}^\dagger + \hat{b}^\dagger)(\hat{a}^\dagger - \hat{b}^\dagger)|0\rangle \\ &= \frac{1}{4}(|\uparrow\rangle + |\downarrow\rangle) \otimes (|\uparrow\rangle + |\downarrow\rangle) \otimes \left[(\hat{a}^\dagger)^2 - (\hat{b}^\dagger)^2\right]|0\rangle.\end{aligned} \tag{SM.12}$$

The state post-scattering is then

$$\begin{aligned}|\psi_3\rangle &= \frac{1}{4}\left(t_1^2(\omega)|\uparrow\rangle + |\downarrow\rangle\right) \otimes (|\uparrow\rangle + |\downarrow\rangle) \otimes (\hat{a}^\dagger)^2 |0\rangle \\ &\quad - \frac{1}{4}(|\uparrow\rangle + |\downarrow\rangle) \otimes \left(t_2^2(\omega)|\uparrow\rangle + |\downarrow\rangle\right) \otimes (\hat{b}^\dagger)^2 |0\rangle.\end{aligned} \tag{SM.13}$$

The state after the second beam-splitter is given by

$$\begin{aligned}|\psi\rangle &= \frac{1}{8}\left[(t_1^2(\omega) - t_2^2(\omega))|\uparrow\uparrow\rangle + (t_1^2(\omega) - 1)|\uparrow\downarrow\rangle + (1 - t_2^2(\omega))|\downarrow\uparrow\rangle + 0|\downarrow\downarrow\rangle\right] \otimes \left[(\hat{a}^\dagger)^2 + (\hat{b}^\dagger)^2\right]|0\rangle \\ &\quad + \frac{1}{4}\left[(t_1^2(\omega) + t_2^2(\omega))|\uparrow\uparrow\rangle + (t_1^2(\omega) + 1)|\uparrow\downarrow\rangle + (1 + t_2^2(\omega))|\downarrow\uparrow\rangle + 2|\downarrow\downarrow\rangle\right] \otimes \hat{a}^\dagger\hat{b}^\dagger|0\rangle.\end{aligned} \tag{SM.14}$$

Making use of projection measurements once again, a measurement outcome heralds one of the following states:

$$|\psi_{(1,0)}\rangle = |\psi_{(0,1)}\rangle = \frac{(t_1^2(\omega) - t_2^2(\omega))|\uparrow\uparrow\rangle + (t_1^2(\omega) - 1)|\uparrow\downarrow\rangle + (1 - t_2^2(\omega))|\downarrow\uparrow\rangle + 0|\downarrow\downarrow\rangle}{\sqrt{[|t_1^2(\omega) - t_2^2(\omega)|^2 + |t_1^2(\omega) - 1|^2 + |1 - t_2^2(\omega)|^2]}} \tag{SM.15}$$

or $\quad |\psi_{(1,1)}\rangle = \frac{(t_1^2(\omega) + t_2^2(\omega))|\uparrow\uparrow\rangle + (t_1^2(\omega) + 1)|\uparrow\downarrow\rangle + (1 + t_2^2(\omega))|\downarrow\uparrow\rangle + 2|\downarrow\downarrow\rangle}{\sqrt{[|t_1^2(\omega) + t_2^2(\omega)|^2 + |t_1^2(\omega) + 1|^2 + |1 + t_2^2(\omega)|^2 + 4]}}.$ $\tag{SM.16}$

We then repeated the probing process and replace the initial state of the emitters with either of the heralded states. Let us consider the system after $N = m + n$ detection events, where m is the number of events where both detectors register a photon and n be the number of events where the two photons reach the same detector. Then we can express the state after the $(N+1)^{\text{th}}$ probe and right before photon-detection as

$$\begin{aligned}|\psi_{m,n}\rangle = \frac{1}{4c_{m,n}}&\Big[(t_1^2(\omega) + t_2^2(\omega))^m(t_1^2(\omega) - t_2^2(\omega))^{n+1}|\uparrow\uparrow\rangle + (1 + t_1^2(\omega))^m(t_1^2(\omega) - 1)^{n+1}|\uparrow\downarrow\rangle \\ &+ (1 + t_2^2(\omega))^m(1 - t_2^2(\omega))^{n+1}|\downarrow\uparrow\rangle\Big] \otimes \left[(\hat{a}^\dagger)^2 + (\hat{b}^\dagger)^2\right]|0\rangle \\ + \frac{1}{2c_{m,n}}&\Big[(t_1^2(\omega) + t_2^2(\omega))^{m+1}0^n|\uparrow\uparrow\rangle + (1 + t_1^2(\omega))^{m+1}(t_1^2(\omega) - 1)^n|\uparrow\downarrow\rangle \\ &+ (1 + t_2^2(\omega))^{m+1}(1 - t_2^2(\omega))^n|\downarrow\uparrow\rangle + 2^{m+1}0^n|\downarrow\downarrow\rangle\Big] \otimes \hat{a}^\dagger\hat{b}^\dagger|0\rangle\end{aligned} \tag{SM.17}$$

where $c_{m,n}$ is the respective normalization constant given by

$$c_{m,n} = \left[\left| (t_1^2(\omega) + t_2^2(\omega))^m (t_1^2(\omega) - t_2^2(\omega))^n \right|^2 + \left| (1 + t_1^2(\omega))^m (t_1^2(\omega) - 1)^n \right|^2 + \left| (1 + t_2^2(\omega))^m (1 - t_2^2(\omega))^n \right|^2 + |2^m 0^n|^2 \right]^{1/2}. \tag{SM.18}$$

Next we justify the limitation placed on the choice of frequency: by selecting a frequency that satisfies $t_1^2(\omega) = t_2^2(\omega)$, (SM.17) simplifies to

$$|\psi_{m,n}\rangle = \frac{1}{4c_{m,n}} \left[(1 + t_1^2(\omega))^m (t_1^2(\omega) - 1)^{n+1} |\uparrow\downarrow\rangle + (1 + t_2^2(\omega))^m (1 - t_2^2(\omega))^{n+1} |\downarrow\uparrow\rangle \right] \otimes \left[\left(\hat{a}^\dagger\right)^2 + \left(\hat{b}^\dagger\right)^2 \right] |0\rangle$$

$$+ \frac{1}{2c_{m,n}} \left[(t_1^2(\omega) + t_2^2(\omega))^{m+1} 0^n |\uparrow\uparrow\rangle + (1 + t_1^2(\omega))^{m+1} (t_1^2(\omega) - 1)^n |\uparrow\downarrow\rangle \right. \tag{SM.19}$$

$$\left. + (1 + t_2^2(\omega))^{m+1} (1 - t_2^2(\omega))^n |\downarrow\uparrow\rangle + 2^{m+1} 0^n |\downarrow\downarrow\rangle \right] \otimes \hat{a}^\dagger \hat{b}^\dagger |0\rangle .$$

Therefore, the choice of frequency allows us to obtain a maximally entangled Bell state $|\Psi^\pm\rangle = (|\uparrow\downarrow\rangle \pm |\downarrow\uparrow\rangle)/\sqrt{2}$ when both photons reach just one detector, or to approach the maximally entangled state $\exp(i\phi)|\uparrow\uparrow\rangle + |\downarrow\downarrow\rangle$. An expression for the relative phase can be obtained by considering how long it takes for the emitters to reach this state: if this state is reached after M consecutive coincident photon-detections, then $\exp(i\phi) = t_1^{2M}(\omega) = t_2^{2M}(\omega)$.

The frequency ω that satisfies the condition $t_1^2(\omega) = t_2^2(\omega)$ is given by either of the following:

$$\hbar\omega = \frac{1}{2} \left[E_1 + E_2 \pm \sqrt{(E_1 - E_2)^2 - \hbar^2 \Gamma_1 \Gamma_2} \right], \tag{SM.20}$$

$$\hbar\omega = \frac{E_2 \Gamma_1 - E_1 \Gamma_2}{\Gamma_1 - \Gamma_2}. \tag{SM.21}$$

General case ($\beta \leq 1$)

We can express the state of the system using the density matrix formalism (this is due to the possibility of obtaining a mixed state post-photon detection), which allows us to obtain a general expression for how the qubits evolve as the probing process is repeated. We choose a frequency that satisfies Eq. (SM.21), where $t_1(\omega) = \pm t_2(\omega)$ no longer holds since γ is no longer zero. Furthermore, it may be the case that the three frequency choices result in different scattering amplitudes for a given emitter pairing, and therefore, in different trajectories. We suppress the scattering amplitude notation so that $t_i(\omega) \to t_i$ and $t_{e,i}(\omega) \to t_{e,i}$.

We start off with an arbitrary density matrix for the qubits, ρ_{emitters}, and a photon in each input arm of the interferometer, $\hat{a}$ and $\hat{b}$:

$$\rho_1 = \rho_{\text{emitters}} \otimes \left[\hat{a}^\dagger \hat{b}^\dagger |0\rangle \langle 0| \hat{a} \hat{b} \right], \tag{SM.22}$$

where

$$\rho_{\text{emitters}} = \begin{matrix} & \begin{matrix} \langle\uparrow\uparrow| & \langle\uparrow\downarrow| & \langle\downarrow\uparrow| & \langle\downarrow\downarrow| \end{matrix} \\ \begin{matrix} |\uparrow\uparrow\rangle \\ |\uparrow\downarrow\rangle \\ |\downarrow\uparrow\rangle \\ |\downarrow\downarrow\rangle \end{matrix} & \begin{bmatrix} c_{11} & c_{12} & c_{13} & c_{14} \\ c_{21} & c_{22} & c_{23} & c_{24} \\ c_{31} & c_{32} & c_{33} & c_{34} \\ c_{41} & c_{42} & c_{43} & c_{44} \end{bmatrix} \end{matrix}. \tag{SM.23}$$

For the first iteration, $c_{ij} = \frac{1}{4}$ for all i, j.

Interacting with the first beamsplitter, where $\hat{a} \to \frac{1}{\sqrt{2}}\left(\hat{a} + \hat{b}\right)$ and $\hat{b} \to \frac{1}{\sqrt{2}}\left(\hat{a} - \hat{b}\right)$, the state evolves to

$$\rho_2 = \rho_{\text{emitters}} \otimes \frac{1}{4} \left[\left(\hat{a}^\dagger\right)^2 - \left(\hat{b}^\dagger\right)^2 \right] |0\rangle \langle 0| [\hat{a}^2 - \hat{b}^2]. \tag{SM.24}$$

The state after the scattering interactions at the emitters is

$$\rho_3 = \frac{1}{4} \sum_{i,j=1,2,3} \rho(M_i, M_j) \otimes \left[M_i \left| 0 \right\rangle \left\langle 0 \right| M_j \right] + \frac{1}{4} \sum_{i,j=1,2,3} \rho(N_i, N_j) \otimes \left[N_i \left| 0 \right\rangle \left\langle 0 \right| N_j \right]$$
$$- \frac{1}{4} \sum_{i,j=1,2,3} \left\{ \rho(M_i, N_j) \otimes \left[M_i \left| 0 \right\rangle \left\langle 0 \right| N_j \right] + \rho(N_i, M_j) \otimes \left[N_i \left| 0 \right\rangle \left\langle 0 \right| M_j \right] \right\}, \tag{SM.25}$$

where

$$M = \begin{bmatrix} \hat{a}^2 \\ \hat{a}\hat{r}_1 \\ \hat{r}_1^2 \end{bmatrix}, \tag{SM.26}$$

$$N = \begin{bmatrix} \hat{b}^2 \\ \hat{b}\hat{r}_2 \\ \hat{r}_2^2 \end{bmatrix}, \tag{SM.27}$$

and where $\hat{r}_i$ is the photon annihilation operator to a reservoir around the emitter in arm i which represents scattering losses, and $\rho(\hat{m}, \hat{n})$ is the respective density matrix of the qubits associated with the scattered optical state $\hat{m}^\dagger \left| 0 \right\rangle \left\langle 0 \right| \hat{n}$. The scattering amplitudes are given by the following transformations:

$$\begin{pmatrix} \left| \uparrow\uparrow \right\rangle \\ \left| \uparrow\downarrow \right\rangle \\ \left| \downarrow\uparrow \right\rangle \\ \left| \downarrow\downarrow \right\rangle \end{pmatrix} \otimes \left(\hat{a}^\dagger \right)^2 \left| 0 \right\rangle \longrightarrow \begin{pmatrix} t_1^2 \left| \uparrow\uparrow \right\rangle \\ t_1^2 \left| \uparrow\downarrow \right\rangle \\ \left| \downarrow\uparrow \right\rangle \\ \left| \downarrow\downarrow \right\rangle \end{pmatrix} \otimes \left(\hat{a}^\dagger \right)^2 \left| 0 \right\rangle + \begin{pmatrix} 2t_1 t_{e,1} \left| \uparrow\uparrow \right\rangle \\ 2t_1 t_{e,1} \left| \uparrow\downarrow \right\rangle \\ 0 \\ 0 \end{pmatrix} \otimes \hat{a}^\dagger \hat{r}_1^\dagger \left| 0 \right\rangle + \begin{pmatrix} t_{e,1}^2 \left| \uparrow\uparrow \right\rangle \\ t_{e,1}^2 \left| \uparrow\downarrow \right\rangle \\ 0 \\ 0 \end{pmatrix} \otimes \left(\hat{r}_1^\dagger \right)^2 \left| 0 \right\rangle, \tag{SM.28}$$

$$\begin{pmatrix} \left| \uparrow\uparrow \right\rangle \\ \left| \uparrow\downarrow \right\rangle \\ \left| \downarrow\uparrow \right\rangle \\ \left| \downarrow\downarrow \right\rangle \end{pmatrix} \otimes \left(\hat{b}^\dagger \right)^2 \left| 0 \right\rangle \longrightarrow \begin{pmatrix} t_2^2 \left| \uparrow\uparrow \right\rangle \\ \left| \uparrow\downarrow \right\rangle \\ t_2^2 \left| \downarrow\uparrow \right\rangle \\ \left| \downarrow\downarrow \right\rangle \end{pmatrix} \otimes \left(\hat{b}^\dagger \right)^2 \left| 0 \right\rangle + \begin{pmatrix} 2t_2 t_{e,2} \left| \uparrow\uparrow \right\rangle \\ 0 \\ 2t_2 t_{e,2} \left| \downarrow\uparrow \right\rangle \\ 0 \end{pmatrix} \otimes \hat{b}^\dagger \hat{r}_2^\dagger \left| 0 \right\rangle + \begin{pmatrix} t_{e,1}^2 \left| \uparrow\uparrow \right\rangle \\ 0 \\ t_{e,2}^2 \left| \downarrow\uparrow \right\rangle \\ 0 \end{pmatrix} \otimes \left(\hat{r}_2^\dagger \right)^2 \left| 0 \right\rangle. \tag{SM.29}$$

The state then interacts with the second beamsplitter, leaving the state of the qubits unaltered and only changing the optical state:

$$\rho_4 = \frac{1}{4} \sum_{i,j=1,2,3} \rho(M_{i,1}, M_{j,1}) \otimes \left[M_{i,2} \left| 0 \right\rangle \left\langle 0 \right| M_{j,2} \right] + \frac{1}{4} \sum_{i,j=1,2,3} \rho(N_{i,1}, N_{j,1}) \otimes \left[N_{i,2} \left| 0 \right\rangle \left\langle 0 \right| N_{j,2} \right]$$
$$- \frac{1}{4} \sum_{i,j=1,2,3} \left\{ \rho(M_{i,1}, N_{j,1}) \otimes \left[M_{i,2} \left| 0 \right\rangle \left\langle 0 \right| N_{j,2} \right] + \rho(N_{i,1}, M_{j,1}) \otimes \left[N_{i,2} \left| 0 \right\rangle \left\langle 0 \right| M_{j,2} \right] \right\}, \tag{SM.30}$$

where M and N now change to

$$M = \begin{bmatrix} \hat{a}^2 & \frac{1}{2}(\hat{a}^2 + 2\hat{a}\hat{b} + \hat{b}^2) \\ \hat{a}\hat{r}_1 & \frac{1}{\sqrt{2}}(\hat{a} + \hat{b})\hat{r}_1 \\ \hat{r}_1^2 & \hat{r}_1^2 \end{bmatrix}, \tag{SM.31}$$

$$N = \begin{bmatrix} \hat{b}^2 & \frac{1}{2}(\hat{a}^2 - 2\hat{a}\hat{b} + \hat{b}^2) \\ \hat{b}\hat{r}_2 & \frac{1}{\sqrt{2}}(\hat{a} - \hat{b})\hat{r}_2 \\ \hat{r}_2^2 & \hat{r}_2^2 \end{bmatrix}. \tag{SM.32}$$

We make use of positive operator-valued measures made up of orthogonal projectors, where $\Pi(\hat{x}) = \hat{x}^\dagger \left| 0 \right\rangle \left\langle 0 \right| \hat{x}$, and assume non-photon-number resolving detectors.

A click by the detector at output arm $\hat{a}$, with no detection in the other detector, is only possible for the projection measurements $\Pi(\hat{a}^2)$, $\Pi(\hat{a}\hat{r}_1)$ and $\Pi(\hat{a}\hat{r}_2)$. This yields the following reduced density matrix for the qubits:

$$
\begin{aligned}
\rho_{(1,0)} &= \frac{1}{P(1,0)} \text{Tr}_{\text{field}} \left[\left(\Pi(\hat{a}^2) + \Pi(\hat{a}\hat{r}_1) + \Pi(\hat{a}\hat{r}_2) \right) \rho_4 \left(\Pi(\hat{a}^2) + \Pi(\hat{a}\hat{r}_1) + \Pi(\hat{a}\hat{r}_2) \right) \right] \\
&= \frac{1}{P(1,0)} \left\{ \frac{1}{16} \left[\rho\left(\hat{a}^2, \hat{a}^2\right) + \rho\left(\hat{b}^2, \hat{b}^2\right) - \rho\left(\hat{a}^2, \hat{b}^2\right) - \rho\left(\hat{b}^2, \hat{a}^2\right) \right] + \frac{1}{8} \left[\rho(\hat{a}\hat{r}_1, \hat{a}\hat{r}_1) + \rho(\hat{b}\hat{r}_2, \hat{b}\hat{r}_2) \right] \right\} \\
&= \frac{1}{P(1,0)} \left(\frac{1}{16} \begin{bmatrix} |(t_1^2 - t_2^2)|^2 & (t_1^2 - t_2^2)(t_1^2 - 1)^* & (t_2^2 - t_2^1)(t_2^2 - 1)^* & 0 \\ (t_1^2 - 1)(t_1^2 - t_2^2)^* & |t_1^2 - 1|^2 & (t_1^2 - 1)(1 - t_2^2)^* & 0 \\ (t_2^2 - 1)(t_2^2 - t_2^1)^* & (1 - t_2^2)(t_1^2 - 1)^* & |t_2^2 - 1|^2 & 0 \\ 0 & 0 & 0 & 0 \end{bmatrix} \right. \\
&\qquad \left. + \frac{1}{8} \begin{bmatrix} |2t_1 t_{e,1}|^2 + |2t_2 t_{e,2}|^2 & |2t_1 t_{e,1}|^2 & |2t_2 t_{e,2}|^2 & 0 \\ |2t_1 t_{e,1}|^2 & |2t_1 t_{e,1}|^2 & 0 & 0 \\ |2t_2 t_{e,2}|^2 & 0 & |2t_2 t_{e,2}|^2 & 0 \\ 0 & 0 & 0 & 0 \end{bmatrix} \right) \circ \rho_{\text{emitters}},
\end{aligned}
\tag{SM.33}
$$

where $\circ$ denotes the Hadamard, or element-wise, product of the two matrices, and ρ_{emitters} is the density matrix of the qubits at the start of the probing round [Eq. (SM.23)]. The probability of obtaining this measurement outcome, $P(1,0)$, is

$$
\begin{aligned}
P(1,0) &= \text{Tr} \left[\left(\Pi(\hat{a}^2) + \Pi(\hat{a}\hat{r}_1) + \Pi(\hat{a}\hat{r}_2) \right) \rho_4 \left(\Pi(\hat{a}^2) + \Pi(\hat{a}\hat{r}_1) + \Pi(\hat{a}\hat{r}_2) \right) \right] \\
&= \frac{1}{16} \left[c_{11}|t_1^2 - t_2^2|^2 + c_{22}|t_1^2 - 1|^2 + c_{33}|t_2^2 - 1|^2 \right] \\
&\quad + \frac{1}{2} \left[c_{11} \left(|2t_1 t_{e,1}|^2 + |2t_2 t_{e,2}|^2 \right) + c_{22}|2t_1 t_{e,1}|^2 + c_{33}|2t_2 t_{e,2}|^2 \right],
\end{aligned}
\tag{SM.34}
$$

where c_{ij} are elements of the emitter density matrix ρ_{emitters}.

For the measurement outcome $(0,1)$, we use the projectors $\Pi(\hat{b}^2)$, $\Pi(\hat{b}\hat{r}_1)$ and $\Pi(\hat{b}\hat{r}_2)$, which gives the same result as for the previous case, i.e., $\rho_{(0,1)}$ is given by Eq. (SM.33) and $P(0,1)$ is given by Eq. (SM.34).

In the case of a coincidence detection, the post-measurement density matrix is given by

$$
\begin{aligned}
\rho_{(1,1)} &= \frac{1}{P(1,1)} \text{Tr}_{\text{field}} \left[\Pi(\hat{a}\hat{b}) \rho_4 \Pi(\hat{a}\hat{b}) \right] \\
&= \frac{1}{4P(1,1)} \left[\rho(\hat{a}^2, \hat{a}^2) + \rho(\hat{b}^2, \hat{b}^2) + \rho(\hat{a}^2, \hat{b}^2) + \rho(\hat{b}^2, \hat{a}^2) \right] \\
&= \frac{1}{4P(1,1)} \begin{pmatrix} |(t_1^2 + t_2^2)|^2 & (t_1^2 + t_2^2)(t_1^2 + 1)^* & (t_1^2 + t_2^2)(t_2^2 + 1)^* & 2(t_1^2 + t_2^2) \\ (t_1^2 + 1)(t_1^2 + t_2^2)^* & |(t_1^2 + 1)|^2 & (t_1^2 + 1)(t_2^2 + 1)^* & 2(t_1^2 + 1) \\ (t_2^2 + 1)(t_1^2 + t_2^2)^* & (t_2^2 + 1)(t_1^2 + 1)^* & |(t_2^2 + 1)|^2 & 2(t_2^2 + 1) \\ 2(t_1^2 + t_2^2)^* & 2(t_1^2 + 1)^* & 2(t_2^2 + 1)^* & 4 \end{pmatrix} \circ \rho_{\text{emitters}},
\end{aligned}
\tag{SM.35}
$$

where

$$
\begin{aligned}
P(1,1) &= \text{Tr} \left[\Pi(\hat{a}\hat{b}) \rho_4 \Pi(\hat{a}\hat{b}) \right] \\
&= \frac{1}{4} \left[c_{11}|(t_1^2 + t_2^2)|^2 + c_{22}|(t_1^2 + 1)|^2 + c_{33}|(t_2^2 + 1)|^2 + 4c_{44} \right].
\end{aligned}
\tag{SM.36}
$$

Note that this reduced matrix represents a pure state.

Finally, we have the case of no photon detection due to scattering losses at the emitters, which results in the state:

$$
\begin{aligned}
\rho_{(0,0)} &= \frac{1}{P(0,0)} \text{Tr}_{\text{field}} \left[\left(\Pi(\hat{r}_1^2) + \Pi(\hat{r}_2^2) \right) \rho_4 \left(\Pi(\hat{r}_1^2) + \Pi(\hat{r}_2^2) \right) \right] \\
&= \frac{1}{4P(0,0)} \begin{pmatrix} |t_{e,1}^2|^2 + |t_{e,2}^2|^2 & |t_{e,1}^2|^2 & |t_{e,2}^2|^2 & 0 \\ |t_{e,1}^2|^2 & |t_{e,1}^2|^2 & 0 & 0 \\ |t_{e,2}^2|^2 & 0 & |t_{e,2}^2|^2 & 0 \\ 0 & 0 & 0 & 0 \end{pmatrix} \circ \rho_{\text{emitters}},
\end{aligned}
\tag{SM.37}
$$

where

$$P(0,0) = \frac{1}{4}\left[c_{11}(|t_{e,1}^2|^2 + |t_{e,2}^2|^2) + c_{22}|t_{e,1}^2|^2 + c_{33}|t_{e,2}^2|^2\right].$$ (SM.38)

The process can now be repeated from Eq. (SM.23), where we replace ρ_{emitters} with one of the four possible resulting qubit density matrices, $\rho_{(i,j)}$, depending on the photon-detection outcome.

Concurrence

We use concurrence to measure the amount of entanglement that is generated between the two qubits: it is an entanglement monotone that can be easily applied to mixed states. The concurrence of two qubits in the state ρ is given by [38]

$$\mathcal{C}(\rho) = \max(0, \lambda_1 - \lambda_2 - \lambda_3 - \lambda_4),$$ (SM.39)

where $\lambda_1, \ldots, \lambda_4$ are the eigenvalues, in decreasing order, of

$$R = \sqrt{\sqrt{\rho}\,(\sigma_y \otimes \sigma_y)\,\rho^*\,(\sigma_y \otimes \sigma_y)\,\sqrt{\rho}}.$$ (SM.40)

In the case of a pure state, $|\psi\rangle = c_1\,|\uparrow\uparrow\rangle + c_2\,|\uparrow\downarrow\rangle + c_3\,|\downarrow\uparrow\rangle + c_4\,|\downarrow\downarrow\rangle$, the concurrence simplifies to

$$\begin{aligned}\mathcal{C}\left(|\psi\rangle\right) &= |\,\langle\psi|\sigma_y \otimes \sigma_y|\psi^*\rangle\,| \\ &= 2|c_1 c_4 - c_2 c_3|.\end{aligned}$$ (SM.41)